Send Orders for Reprints to reprints@benthamscience.ae

100 *Current Alzheimer Research,* 2015, *12,* 100-115

Age-Dependent Biochemical Dysfunction in Skeletal Muscle of Triple-Transgenic Mouse Model of Alzheimer`s Disease

Vera F. Monteiro-Cardoso[1,#], Marisa Castro[1,#], M.M. Oliveira[1], Paula I. Moreira[2,3], Francisco Peixoto[4] and Romeu A.Videira[1,*]

[1]*Chemistry Center - Vila Real (CQ-VR), Chemistry Department, School of Life and Environmental Sciences, University of Trás-os-Montes e Alto Douro, UTAD, P.O. Box 1013; 5001-801 Vila Real, Portugal;* [2]*Laboratory of Physiology, Faculty of Medicine, University of Coimbra, 3000-548 Coimbra, Portugal;* [3]*CNC - Center for Neuroscience and Cell Biology, University of Coimbra, 3004-517 Coimbra, Portugal;* [4]*Centre for the Research and Technology of Agro-Environmental and Biological Sciences (CITAB), Department of Biology and Environment, School of Life and Environmental Sciences, UTAD, P.O. Box 1013; 5001-801 Vila Real, Portugal*

Romeu A.Videira

Abstract: The emergence of Alzheimer`s disease as a systemic pathology shifted the research paradigm toward a better understanding of the molecular basis of the disease considering the pathophysiological changes in both brain and peripheral tissues. In the present study, we evaluated the impact of disease progression on physiological relevant features of skeletal muscle obtained from 3, 6 and 12 month-old 3xTg-AD mice, a model of Alzheimer`s disease, and respective age-matched nonTg mice. Our results showed that skeletal muscle functionality is already affected in 3-month-old 3xTg-AD mice as evidenced by deficient acetylcholinesterase and catalase activities as well as by alterations in fatty acid composition of mitochondrial membranes. Additionally, an age-dependent accumulation of amyloid-β_{1-40} peptide occurred in skeletal muscle of 3xTg-AD mice, an effect that preceded bioenergetics mitochondrial dysfunction, which was only detected at 12 months of age, characterized by decreased respiratory control ratio and ADP/O index and by an impairment of complex I activity. HPLC-MS/MS analyses revealed significant changes in phospholipid composition of skeletal muscle tissues from 3xTg-AD mice with 12 months of age when compared with age-matched nonTg mice. Increased levels of lyso-phosphatidylcholine associated with a decrease of phosphatidylcholine molecular species containing arachidonic acid were detected in 3xTg-AD mice, indicating an enhancement of phospholipase A_2 activity and skeletal muscle inflammation. Additionally, a decrease of phosphatidylethanolamine plasmalogens content and an increase in phosphatidylinositol levels was observed in 3xTg-AD mice when compared with age-matched nonTg mice. Altogether, these observations suggest that the skeletal muscle of 3xTg-AD mice are more prone to oxidative and inflammatory events.

Keywords: Alzheimer's disease, amyloid-β, lipidomics, mitochondrial bioenergetics, phospholipase A_2, phospholipids, skeletal muscle.

INTRODUCTION

Alzheimer`s disease is the most common progressive neurodegenerative disease affecting millions of people worldwide. The Alzheimer's brain is marked by neurodegeneration, comprising loss of synapses and neurons particularly in areas associated with memory and learning. The extracellular deposition of amyloid-β peptide and intracellular formation of neurofibrillary tangles are other consistent inscriptions in the brains of patients affected by the disease [1]. Simultaneously with these brain pathological hallmarks, an abnormal metabolism of amyloid precursor protein (APP) with amyloid-β deposition in non-neuronal tissues (e.g. skeletal muscle) were detected in both human and animal models of Alzheimer`s disease [2, 3]. Additionally, Alzheimer's patients exhibit frequently a progressive decline in muscle strength and activity associated with a great reduction in skeletal muscle mass, which contribute to the disability and loss of functional independence of the individuals [4]. In fact, abnormal body weight loss and cachexia are clinical features of Alzheimer`s disease patients [5]. Although the causes underlying body weight loss remain unknown, experimental data indicated that progressive brain atrophy and the cognitive shortfall in Alzheimer's patients are positively correlated with the loss of muscular mass suggesting that dysfunctions in brain and skeletal muscle may emerge from common mechanisms [4]. Therefore, it was postulated that Alzheimer`s disease may be associated with a deficiency in the regulation of energy metabolism [6, 7]. In fact, the loss of the homeostatic control of energy metabolism due to mitochondrial dysfunction has been implicated as the common cause underling both brain and skeletal muscle dysfunctions detected in Alzheimer`s disease subjects [8, 9].

*Address correspondence to this author at the Chemistry Center - Vila Real (CQ-VR), Chemistry Department, School of Life and Environmental Sciences, University of Trás-os-Montes e Alto Douro, UTAD, P.O. Box 1013; 5001-801 Vila Real, Portugal; Tel:+351 259350273; Fax: +351 259350480; E-mail: rvideira@utad.pt

[#]*These authors contributed equally to this work*

1875-5828/15 $58.00+.00

The progressive atrophy and depletion of cholinergic system is another important inception of Alzheimer's pathophysiology as supported by human postmortem brain analyses and by *in vivo* studies using advanced imaging techniques [10-13]. Depressed acetylcholinesterase (AChE) activity in brain cortical regions and the atrophy of the nucleus basalis of Meynert (the main source of the cholinergic neurotransmitter acetylcholine) were correlated with cognitive deficits measured by dementia rating scales in Alzheimer's patients [14]. In fact, the recognition of a progressive decline in brain acetylcholine levels [15, 16] led to the use of AChE inhibitors as valuable therapeutic agents for Alzheimer's disease treatment [17].

Although AChE inhibitors (e.g. tacrine and analogs) increase cholinergic transmission, these compounds have modest and transient therapeutic effects [18]. The weak therapeutic benefits obtained with AChE inhibitors should result from the combination of several factors, including their brain toxic effects emerging from changes in lipid composition of mitochondria with significant cellular bioenergetics repercussions [19], and the impairment of other acetylcholine-mediated biological functions besides its involvement in cholinergic neurotransmission [20]. It is noteworthy that AChE exist in both cholinergic and non-cholinergic brain areas, being present in different oligomerization states or molecular forms (tetramers, dimers and monomers) and exhibiting cell-specific expression patterns [21]. Alzheimer's disease progression is associated with the selective loss of AChE tetramers preserving or even increasing the levels of dimeric and monomeric forms [22, 23], which are apparently correlated with tau hyperphosphorylation and amyloid-beta overproduction [24-26]. Additionally, overall AChE activity in Alzheimer's brains appears to be slightly decreased than in age-matched control brains, as demonstrated by studies in both human and animal models [27, 28]. On the other hand, the globular tetramers of AChE are bound to plasma membrane [29], and consequently their stability and activity is modulated by the biophysical properties of host membranes which are dependent of lipid composition. Therefore, the cholinergic system may be also perturbed by changes in lipid composition of the cell membranes where AChE is attached (e.g. neurons and skeletal muscles cells). In fact, changes in lipid profile of brain cell membranes were detected and considered as a characteristic feature of Alzheimer`s phenotype [30, 31].

Considering the relevance of cholinergic system in regulating muscle activity, it is expected that skeletal muscle dysfunction associated with abnormal body weight loss detected in Alzheimer's patients may result from anabnormal regulation of the cholinergic system. In this study we used the triple transgenic mouse model of Alzheimer's disease (3xTg-AD) in order to analyze the pathophysiological impact of the disease progression on skeletal muscle functionality by focusing three aspects: i) AChE activity; ii) redox state of muscle cells by evaluating superoxide dismutase (SOD) and catalase activities and total sulfhydryl content; iii) mitochondrial bioenergetics activity and its putative relationship with fatty acid profile changes. Additionally, the phospholipid profile of skeletal muscle tissue was evaluated in animals with 12 months of age that already exhibit the brain pathological hallmarks of the disease, deposits of amyloid-β peptide and neurofibrillary tangles.

MATERIAL AND METHODS

Animal Care

Animal experiments were conducted according to the National (DL 129/92; DL 197/96; P 1131/97) and European Convention for the Protection of Animals used for Experimental and Other Scientific Proposes and related European Legislation (2010/63/EU). Male nontransgenic (nonTg; C57BL6/129S) and triple transgenic (3xTg-AD) mice for Alzheimer's disease were obtained from the Center for Neuroscience and Cell Biology (CNC) Animal Facility, University of Coimbra. Animals were bred and maintained at the Veterinary Hospital of the University of Trás-os-Montes e Alto Douro and were housed in polycarbonate cages on a 12 h light/dark cycles. Room temperature was maintained at 24±2 ºC with relative humidity 55±5%. Food and water were provided *ad libitum.* The characterization of amyloid and tau pathologies has been described previously in this model [32] and confirmed regularly in our colony. In the present work male mice with 3 (pré-synptomatic age), 6 (emergence of amyloid-β pathology) and 12 (emergence of tau pathology) months-old were used, considering the following experimental design: in each time point, each n corresponds to 3 animals with same age, coming from 3 distinct litters. Thus for this study were required nine litters and, at least, 3 mice of each one were used (1 grown until 3 months of age, 1 grown until 6 months of age and 1 grown until 12 months of age) in order to minimize the effects of the genomic diversity within each group.

Determination of Acetylcholinesterase (AChE) Activity in Skeletal Muscle

Mitochondria-free cytosolic fractions were obtained from nonTg and 3xTg-AD skeletal muscle after tissue homogenization and centrifugation at 16000 x *g* for 20 minutes at 4 ºC (Sigma 2K-16). The pellet was discharged and the supernatant (mitochondria-free cytosolic fraction) was used for the enzymatic assays. The protein concentration of supernatants was determined by the biuret method using bovine serum albumin as a standard [33]. AChE activity was evaluated as function of substrate concentration, using seven concentrations of acetylthiocholine iodide, to determine the Michaelis-Menten kinetic parameters Km (Michaelis constant) and V_{max} (maximal velocity), as previously described [19].

Amyloid-β_{1-40} Enzyme-Linked Immunosorbent Assay (ELISA)

Amyloid-β_{1-40} levels were quantified in mitochondria-free cytosolic fractions using Human amyloid-β_{1-40} ELISA kit (Invitrogen). Mitochondria-free cytosolic fractions were obtained from skeletal muscle homogenates as described above (see AChE activity) supplemented with a protease inhibitors cocktail (SIGMA-ALDRICH). Mitochondria-free cytosolic fractions were diluted (1:2, v/v) in an appropriate Standard Diluent Buffer provided by the manufacturer and supplemented with AEBSF (Protease Inhibitor Cocktail Set I, Calbiochem, La Jolla, CA). The following steps of ELISA were

performed according to manufacturer's protocol. The absorbance was read at 450 nm and the concentrations in the muscle samples were calculated from standard curves. Results were expressed as pg/ mg of protein.

Determination of Enzymatic Antioxidant Defenses and Total Sulfhydryl Content

Skeletal muscle antioxidant enzymatic defenses (SOD and catalase) and total sulfhydryl groups content were evaluated in mitochondria-free cytosolic fractions from nonTg and 3xTg-AD mice skeletal muscle.

Copper-zinc SOD (CuZn-SOD) activity was evaluated using 0.5 mg of protein into phosphate buffer (50 mM KH_2PO_4, 1mM EDTA, pH 7.4) supplemented with 0.1 mM nitro blue tetrazolium (NBT) and 0.1 mM hipoxantine [34]. Absorbance was measure in a Cary 50 UV-Vis spectrophotometer (Agilent Technologies, Santa Clara, CA, USA) at 560 nm after adding 0.023 U mol^{-1} xanthine oxidase. The values were expressed as U act/mg protein in which U expresses the enzyme activity that inhibit the reduction of NBT to blue formazan by 50%.

Catalase activity was determined polarographically following the oxygen production using a Clark-type oxygen electrode (Hansatech, Norfolk, UK) resulting from H_2O_2 decomposition [35]. The reaction was conducted in 1 mL of 50 mM sodium phosphate buffer (pH 7.0) supplemented with 0.1 mg of protein and initiated by adding 1 M H_2O_2. Catalase activity was expressed in terms of nmol O_2 produced per minute per milligram protein.

Total sulfhydryl content (protein SH groups and reduced glutathione, GSH) was evaluated spectrophotometrically using 5,5'-dithiobis (2-nitrobenzoic acid) (DTNB, Elman's reagent Reagent), as previously described [36]. Samples (0.3 mg of protein) were incubated at room temperature in 2 mL of phosphate buffer (100 mM potassium phosphate, pH 8.0) supplemented with DTNB reagent (5 mM) for 15 minutes. Then, the absorbance of the produced yellow-colored thiolate, 5-thio-2-nitrobenzoic acid (TNB), was evaluated at 412 nm, using a Cary 50 UV-Vis spectrophotometer (Agilent Technologies, Santa Clara, CA, USA). The total sulfhydryl content in samples was calculated using a standard curve prepared with different concentration of GSH (0 and 250 μM), which underwent the same sample treatment. The values were expressed as moles of GSH equivalents per milligram of protein.

Skeletal Muscle Mitochondria Isolation and Mitochondrial Respiration

Mitochondria were isolated from skeletal muscle homogenates from nonTg and 3xTg-AD mice by differential centrifugation, as previously described [37], with some modifications. Briefly, intercostal and leg skeletal muscles were quickly removed, cut in small pieces and incubated for 3 minutes with 0.15 mg/ml trypsin from bovine pancreas (Type I sibma 8003) and then homogenized at 4 ºC in isolation medium (250 mM sucrose, 5mM HEPES, 0.2 mM EGTA, 0.1 mM EDTA, pH 7.4). Skeletal muscle homogenates were centrifuged at 12000 x *g* for 10 minutes at 4 ºC (Sigma 2K-16). The pellet was recovered, resuspended in BSA enriched medium (250 mM sucrose, 5 mM HEPES, 0.2 mM EGTA, 0.1 mM EDTA, 0,2% BSA, pH 7.4) and centrifuged at 800 x*g* for 10 minutes. The supernatant was filtered through a gauze and centrifuged at 12000 x *g* for 10 minutes. Mitochondrial pellet was then re-suspended in washing medium (250 mM sucrose, 5 mM HEPES, 1 mM ATP, pH 7.4) and re-centrifuged at 12000 x *g* for 10 minutes. Total protein content of samples was determined by the Biuret method [33]. Oxygen consumption of fresh skeletal muscle mitochondria was monitored polarographically with a Clark-type oxygen electrode (Hansatech, Norfolk, UK). The assays occurred at 30 ºC in 1 mL of reaction buffer containing 130 mM sucrose, 50 mM KCl, 5 mM $MgCl_2$, 5 mM KH_2PO_4 and 5 mM HEPES, at pH 7.2, and supplemented with 1 mg of mitochondrial protein. Mitochondria were energized with 5 mM pyruvate/5 mM malate. ADP (100 nmol/mg of protein) was added to initiate state 3 respiration. After ADP phosphorylation respiration enter in a resting state (state 4 respiration). Oxygen consumption was expressed as nmol O_2/min./mg of protein. Respiratory control ratio (RCR) is defined as the ratio of state 3 to state 4 respiratory rates. ADP/O index is expressed by the ratio between the amount of ADP added and oxygen consumed during respiratory state 3.

Determination of Adenine Nucleotide Levels

At the end of each respiration assay, 500 μL of 0.3 M perchloric acid were added into 500 μL of each sample and then centrifuged at 16000 x *g* for 10 minutes. Resulting supernatants were neutralized by adding 1 M KOH in 5 mM Tris and again centrifuged at 16000 x *g* for 2 minutes. Supernatants were filtered into a new tubes and analyzed. Adenine nucleotide levels were accessed by separation in a reverse phase high performance liquid chromatography (HPLC) through a Lichrospher 100 RP 18 (5 μm) column in a Beckman-System Gold. An isocratic elution with 100 mM phosphate buffer (KH_2PO_4; pH 6.5) supplemented with 1.2% methanol was performed with a flow rate of 1 ml/min and the detection wavelength was set at 254 nm, as previously described [38].

Mitochondrial Respiratory Chain Complexes Activities

All assays were carried out using 0.3 mg of mitochondrial protein on a controlled temperature (30 ºC) according to previously described methods [39]. Complexes I, II, IV and F_oF_1-ATPase activities were normalized to citrate synthase activity (CS) which was performed at 412 nm following the reduction of DTNB (OD 13600 M^{-1} cm^{-1}) in a buffer containing 200 mM Tris-HCl, pH 8.0, 0.01 mM DTNB, 0.02% Triton X-100, 1 mM oxaloacetate and 0.37 mM Acetil-CoA. Briefly, complex I (NADH: ubiquinone oxidoreductase) activity was monitored following the oxidation of NADH in a Varian Eclipse fluorescence spectrophotometer (Agilent Technologies, Santa Clara, CA, USA) at 450 nm, setting excitation at 366 nm. The assay buffer consisted of 25 mM KH_2PO_4, 10 mM $MgCl_2$, pH 7.4, supplemented with 1 mM KCN and 50 μM NADH. The reaction was initiated by adding 162.5 μM decylubiquinone. The enzyme activity was determined by the difference between the slopes before and after 3.0 μM rotenone (specific com-

plex I inhibitor) addition. This value was expressed in arbitrary units/min./mg. Complex II (succinate dehydrogenase) activity was monitored at 600 nm by following the reduction of 6,6-dichlorophenolindophenol (DCPIP) (OD 19100 M^{-1} cm^{-1}) in potassium phosphate buffer (25 mM, pH 7.4) containing, 2 mM KCN, 6.5 µM rotenone, 6.5 µM antimycin *A*, 0.05 mM DCIP and 0.1 mM decylubiquinone. The reaction was initiated by adding 20 mM succinate and stopped 5 minutes later by adding 0.5 mM oxaloacete (complex II inhibitor). Complex IV (Cytochrome *c* oxidase) activity was determined evaluating oxygen consumption in a Clark-type oxygen electrode (Hansatech, Norfolk, UK) in 1 mL standard a buffer (130 mM sucrose, 50 mM KCl, 5 mM $MgCl_2$, 5 mM KH_2PO_4 and 5 mM HEPES, pH 7.2) supplemented with 3 µM rotenone, 0.1 µM antimycin A (inhibitor of complex III) and 15 µM cytochrome *c*. Oxygen consumption was stopped by adding 2 mM KCN (specific inhibitor of complex IV) and specific complex IV activity was expressed as nmol O_2/min./mg protein. F_oF_1-ATPase activity was evaluated by measuring the pH changes associated with transmembrane proton translocation resulting from ATP hydrolysis in a Kipp and Zonen recorder (Omni Instruments, Dundee, UK). The assay buffer (130 mM sucrose, 60 mM KCl, 0.5 mM Hepes and 2.5 mM $MgCl_2$, pH 7.0) was supplemented with 3 µM rotenone and the reaction was initiated by adding 2 mM ATP-Mg. At the end, a standard solution of HCl was used to calibrate the assay. Only the oligomycin (2 µg/mg mitochondrial protein) sensitive rate was considered.

Lipid Extraction and Phospholipid Quantification

Phospholipids extraction was performed according to Bligh and Dyer method with some modifications, as previously described [39], using a solvent combination of methanol/chloroform/water (2:1:0.8, v/v/v) and then phospholipid content was determined according to the method outlined by Bartlett and Lewis [40]. In brief, lipid samples (50 - 100 µL) were incubated at 180 ºC for 2 h with 0.65 mL of concentrate perchloric acid (70%, w/v). After cooling down 3.3 mL of H_2O, 0.5 mL of 1% (w/v) ammonium molybdate and 4% (w/v) ascorbic acid were added to all samples, followed by incubation at 100 ºC for 10 minutes in a water bath. Absorbance was then measured at 800 nm in a Varian Cary 50 spectrophotometer. Phosphorous concentration in each sample was determined using standards ranging from 0 to 250 nmol phosphate.

Preparation of Fatty Acid Methyl Esters

Fatty acid methyl ester (FAME) from mitochondrial lipid extract was obtained by acid catalyzed transmethylation [41]. The mitochondrial lipid extract (400-900 nmol) was dissolved in 5 mL 5 % (v/v) of HCL in methanol (freshly prepared) and 10 mM $C_{17:0}$ was used as internal standard. The mixture was vigorously vortexed for 1 minute and incubated at 70 °C for 120 minutes. After cooling down, 5 mL n-hexane were added and mixed followed by centrifugation at 2000 x *g* for 5 minutes. The organic phase (hexane containing FAME) was collected, dried with Na_2SO_4 anhydrous, filtered and evaporated under a stream of nitrogen. The dry residue was solubilized in a small volume of n-hexane.

Fatty Acid Composition Analysis

The hexane FAME solution was analyzed by Gas Chromatography (GC), using a Thermo Finningan-Trace Gas Chromatograph connected to the mass spectrometer Polaris Q MSn equipped with an Ion Trap analyzer. The column used was a Supelcowax 10 M (30 m, 0.32 mm I.D., 0.50 mm film thickness, 0.45 mm O.D.) from Supelco, Bellefonte, Pennsylvania, USA. Injections were made in splitless mode (1 minute) with an injection volume of 1 mL. The column oven temperature was settled at an initial value of 140 °C (1 min hold), increased to 240 °C with a ramp of 2.0 °C/minutes (9 minutes hold), and finally increased to 280 °C with a ramp of 4.0 °C/minute. Total runtime was 70 minutes using Helium as the carrier gas, at a constant flow of 1 mL/minute. The injector temperature was set at 250 °C. Data acquisition and treatment of results were carried out with an Xcalibur data system (V2.0, ThermoFinnigan, San Jose, CA, USA). Fatty acids were identified by comparison with retention time and fragmentation profile of reference standard mixtures FAME 37 (Supelco 37 Component FAME Mix) and quantified using the peak area of the internal standard. The peroxidability index and un-saturation index (UI) were calculated as previously described [41].

Separation of Phospholipids Classes by Thin-Layer Chromatography (TLC)

TLC was used to separate phospholipid classes present in the lipid crude extracted from homogenized skeletal muscle tissue of mice with 12 months of age. Before use, silica plates were washed with chloroform/methanol (1:1, v/v) and treated with 2.3% (w/v) boric acid in ethanol. The plates with spots containing between 20 and 30 µg of phosphorous were developed in solvent mixture chloroform/ethanol/water/triethylamine (35:30:7:35, v/v/v/v). Lipid spots were visualized with a UV lamp (λ=254 nm) after primuline (50 µg/100 mL in acetone/water, 80:20; v/v) detection. Phospholipid classes present in each TLC spot was identified by phospholipid standards comparison, scraped off the plates to proceed to lipid extraction and quantification. Additionally, cardiolipin (CL) lipid extracts from TLC spots were directly analyzed by ESI-MS in negative mode in an electrospray linear ion trap mass spectrometer (ThermoFinnigan, San Jose, CA, USA), following the conditions indicated below for lipid analysis in negative ion mode. CL MS analysis were performed in three independent samples.

Separation and Quantification of Phospholipid Classes by High Pressure Liquid Chromatography - Mass Spectrometry (HPLC-MS)

Characterization of individual molecular species within each phospholipid class was achieved by mass spectrometry after separation by liquid chromatography using an HPLC-MS system (ThermoFinnigan, San Jose, CA, USA) and Luna column (150 × 2.0 mm, 3 µm; Phenomenex). The mobile phase A consisted of 10% water, 10% chloroform, 45% acetonitrile and 35% methanol (v/v). The mobile phase B consisted of 50% acetonitrile, 10% chloroform, 40% methanol with 10 mM amonium acetate. Solvents gradient started with 100% of phase A followed by a linear decrease to 100% of phase B during 20 minutes, and held isocratically for 35

minutes, returning to the initial conditions in 5 minutes. The flow rate through the column was 200 µL/minutes obtained using a pre-column split (Acurate, HPLC Packings, USA). Mass electrospray analysis was done using the following parameters: source voltage, 5 kV, positive mode, 4.7 kV, negative mode, source temperature, 285 ºC, sheath gas flow, 8 U, source current, 100 ua, capillary voltage, 10 V, positive mode, -43 V negative mode. An isolation with of 0.5 Da was used with a 30-ms activation time for MS/MS experiments. Data acquisition and treatment of results were carried out with an Xcalibur data system (V2.0, Thermo Finnigan, San Jose, CA, USA). Quantitation of individual molecular phospholipid species were calculated by determining the ratio of the peak area of each molecular specie to the corresponding internal standard added to samples prior to lipid extraction. Phospholipid internal standards were used with fatty acid chains as follows: phosphotidylcholine, PC (14:1/17:0); sphingomielyn, SM (d18:1/12:0); phosphatidylinositol, PI (14:1/17:0); phosphatidylethanolamine, PE (14:1/17:0); phosphatidic acid, PA (14:1/17:0); phosphatidylserine, PS (14:1/17:0) and CL ($(15:0)_3$/16:1), all obtained from Avanti polar lipids.

Statistical Analysis

All the data presented in this study correspond to the mean value of n experiments ± SD, with n≥3. Data sets were analyzed by one-way ANOVA test with Student-Newman-Keuls *post hoc* comparisons. Statistical significance was attained at $p<0.05$.

RESULTS

AChE Activity in Skeletal Muscle Tissue

Fig. (**1**) shows the AChE activity in mitochondria-free cytosolic fractions prepared from skeletal muscle of nonTg and 3xTg-AD mice with 3 (Fig. **1A**), 6 (Fig. **1B**) and 12 (Fig. **1C**) months of age, as function of substrate concentration, which follows a Michaelis-Menten kinetics equation, with the values of apparent kinetic parameters (Km and V_{max}) as function of age displayed in Fig. (**1D** and **E**), respectively. The Michaelis-Menten kinetic equation fits reasonably well with the experimental data as reflected by low $\chi 2$ values, approaching zero, and high correlation factors (R) (Supplementary Table **1**). Although Km values are similar in both groups, V_{max}values obtained for 3xTg-AD mice are signifi-

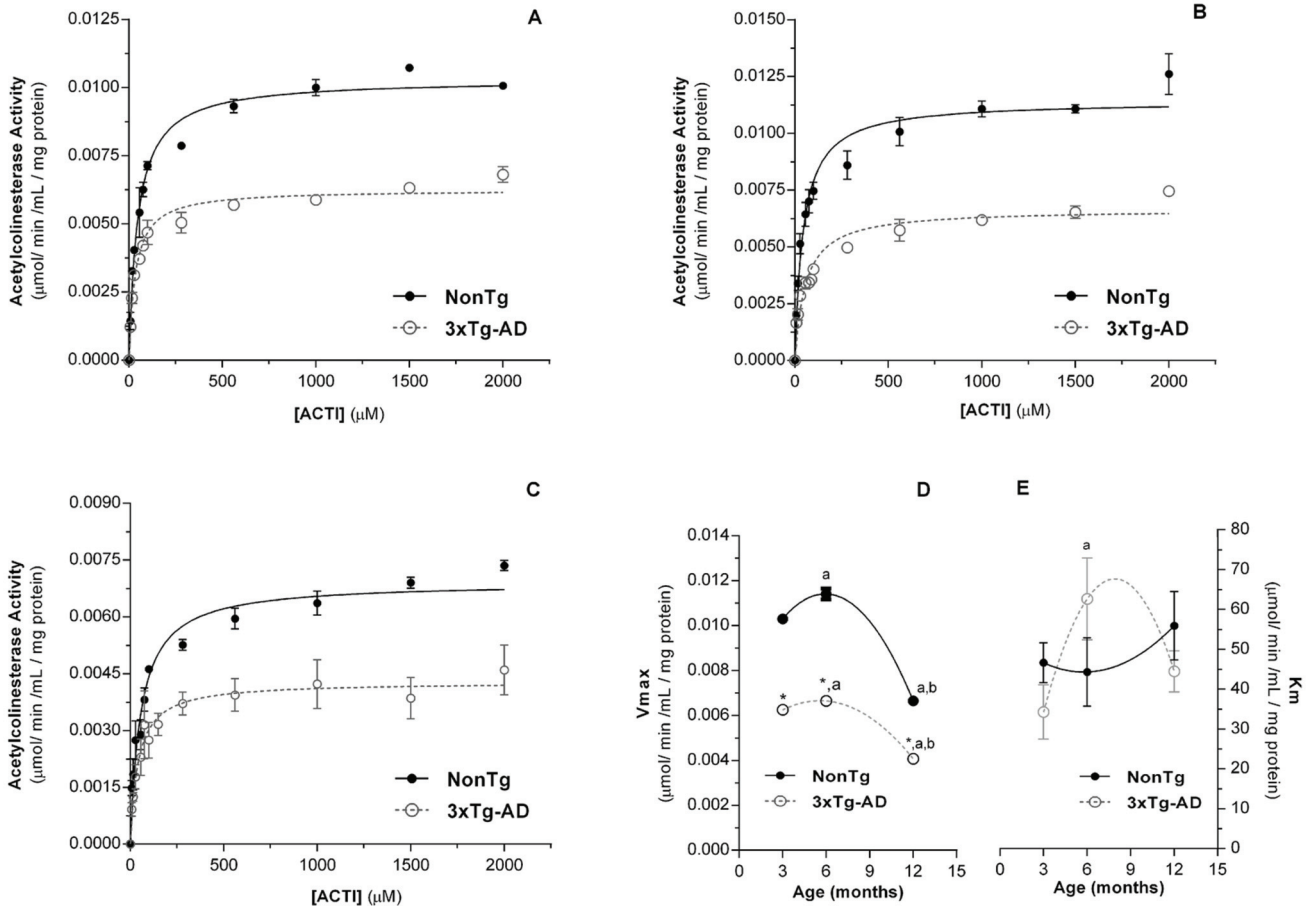

Fig. (1). Acetylcholinesterase (AChE) activity in skeletal muscle homogenates from nonTg (dark circles) and 3xTg-AD (open circles) muscle from mice with 3 (**A**), 6 (**B**) and 12 (**C**) months of age. AChE data were fitted into a Michaelis-Menten kinetic equation. Error-minimization procedure with a $\chi 2$ between successive iterations of ≤0.001%. V_{max} (**D**) and Km (**E**) apparent Michaelis-Menten kinetic parameters of muscle AChE of nonTg and 3xTg-AD groups. Error bars represent standard deviation for 3 independent experiments using 3 animals in each one. * Significantly different from nonTg group, with $p\leq0.05$. ^{a,b} Significantly different from 3 and 6 months of age, respectively, with $p\leq0.05$.

cantly lower than those obtained with age-matched nonTg mice (Fig. **1**). These results suggest that even though the maximal skeletal muscle AChE capacity to hydrolyze acetylcholine is decreased by the pathological situation, the substrate's affinity by the enzyme is preserved. Considering the aging effects on the AChE kinetic parameters, it is evident in both nonTg and 3xTg-AD mice that V_{max} suffer a slight increase between 3 and 6 months of age followed by a pronounced decrease at 12 months of age. Curiously, the maximal capacity of the skeletal muscle AChE to hydrolyze acetylcholine exhibited by nonTg mice with 12 months of age is similar to that exhibited by 3xTg-AD mice with 6 months of age (Fig. **1**).

Table 1. Amyloid-$\beta_{1\text{-}40}$ levels in mitochondria-free cytosolic fractions obtained from skeletal muscle homogenates of nonTg and 3xTg-AD mice

	3 Months	6 Months	12 Months
NonTg (pg/mg of protein)	46.11±8.20	57.38±7.92	56.44±10.45
3xTg-AD (pg/mg of protein)	44.47±11.60	138.02±30.35*	241.31±35.80**

Results are expressed as mean±std of three independent experiments using 3 animals in each one. *, ** Significantly different from nonTg group, with p≤0.05 and p≤0.01, respectively.

Enzymatic Antioxidant Defenses and Total Sulfhydryl Content in Skeletal Muscle Tissue

SOD and catalase activities and total sulfhydryl groups content were evaluated in skeletal muscle mitochondria-free cytosolic fractions of nonTg and 3xTg-AD mice with 3, 6 and 12 months of age in order to assess the impact of aging and Alzheimer`s disease evolution on oxidative changes in skeletal muscle tissue. As shown in Fig. (**2**), SOD activity as well as the total sulfhydryl groups in skeletal muscle cytosolic fractions obtained from nonTg and 3xTg-AD mice are similar for the three ages under study. On the other hand, catalase activity in 3xTg-AD mice are significantly decreased (at least of 50%) when compared with age-matched controls. Even though these data may suggest that 3xTg-AD mice have an increased susceptibility to oxidative stress due to lower antioxidant enzymatic activity, total sulfhydryl groups (that include SH groups of proteins and GSH) content analyses ruled out an accumulation of oxidative damage in skeletal muscle proteins associated to disease progression. Aging effects on SOD and catalase are reflected in the significant increase in the activity of these enzymes, particularly evident between 3 and 6 months of age, where SOD and catalase activities increased more than 2 fold in nonTg group and about 2 and 1.8 fold, respectively, in 3xTg-AD group. Regarding reactive sulfhydryl groups content, it is detected an age-dependent decrease, reaching statistical significance at 12 months of age in both nonTg and 3xtg-AD mice (Fig. **2**).

Amyloid-$\beta_{1\text{-}40}$ Peptide in Skeletal Muscle Tissue

The accumulation of amyloid-$\beta_{1\text{-}40}$ peptide in skeletal muscle of both Alzheimer`s disease patients and animal models has been considered an important feature of abnormal APP metabolism in peripheral tissues [9, 42]. Thus, we evaluated the amyloid-$\beta_{1\text{-}40}$ levels in skeletal muscle using ELISA specifically for human amyloid-$\beta_{1\text{-}40}$ in nonTg and 3xTg-AD mice with 3, 6 and 12 months of age. As shown in (Table **1**), skeletal muscle amyloid-$\beta_{1\text{-}40}$ levels increase with age in 3xTg-AD mice reaching statistical significant differences at 6 and 12 months of age compared to age-matched nonTg mice. In contrast, nonTg mice do not present an age-dependent alteration in amyloid-$\beta_{1\text{-}40}$ levels. Although brain presence of both senile plaques (amyloid-β pathology) and neurofibrillary tangles was confirmed by immunohistochemistry in animals with 14 months of age coming from a litter used in this work [43], our immunohistochemistry assays did not allow to confirm their presence in skeletal muscle tissue (data not shown).

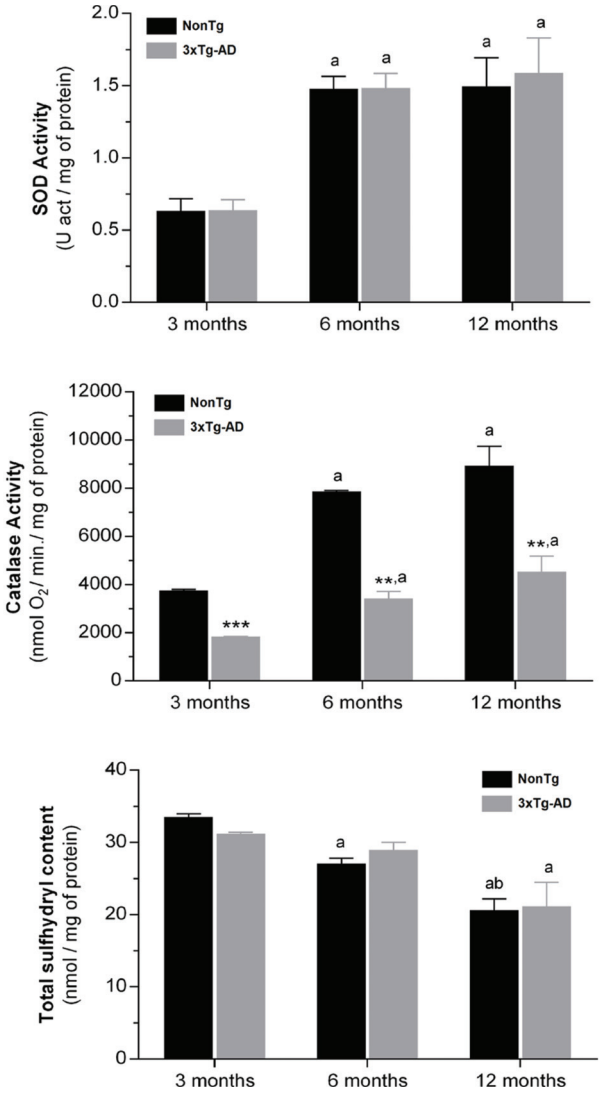

Fig. (2). SOD and catalase activities and total sulfhydryl content (protein SH groups and reduced glutathione) in the skeletal muscle homogenates from nonTg (black bars) and 3xTg-AD (gray bars) mice with 3, 6 and 12 months of age. Error bars represent standard deviation for n≥3 independent experiments. **, *** Significantly black bars different from nonTg group, with p≤0.01 and p≤0.001, respectively. a, b Significantly different from 3 and 6 months of age, respectively, with p≤0.05.

Table 2. Mitochondrial respiratory parameters.

	3 Months		6 Months		12 Months	
	NonTg	**3xTg-AD**	**NonTg**	**3xTg-AD**	**NonTg**	**3xTg-AD**
State 3 (nmol O_2/min./mg of protein)	18.18±3.26	17.40±2.75	25.38±3.8	24.22±3.52	29.52±3.28	26.15±3.03
State 4 (nmol O_2/min./mg of protein)	3.82±0.45	4.20±0.70	4.26±0.61	4.12±0.48	4.89±0.61	6.38±0.51
RCR	4.75±1.01	4.14±0.94	5.90±1.24	5.87±1.09	6.03±1.00	4.09±0.58*
ADP/O (nmol ADP/nATgO/min./mg of protein)	1.41±0.40	1.29±0.38	2.07±0.49	1.97±0.44	2.41±0.40	1.94±0.27*
ATP (nmol/mg of protein)	92.53±7.67	102.92±13.07	92.46±7.24	88.82±13.67	88.76±4.37	78.42±2.79*
ADP (nmol/mg of protein)	15.73±2.67	16.99±3.39	16.42±1.25	16.48±1.38	13.94±1.27	20.59±1.19*

Results are expressed as mean±std of three independent experiments using 3 animals in each one. ATP and ADP levels determined in the final of respiratory assays.* Significantly different from nonTg group, with $p \leq 0.05$.

Skeletal Muscle Mitochondrial Bioenergetics

The mitochondrial respiration was stimulated by adding pyruvate/malate and ADP to determine the ADP-stimulated respiration rate (state 3), while state 4 respiration rate was assessed after total ADP phosphorylation. Oxygen consumption rate in state 3 and state 4, RCR and ADP/O ratios as well as ATP and ADP levels are shown in (Table **2**). In 3xTg-AD group, only at 12 months of age skeletal muscle mitochondria exhibit lower RCR (nonTg 6.03±1.00, 3xTg-AD 4.09±0.58) and ADP/O (nonTg 2.41±0.40, 3xTg-AD 1.94±0.27) ratios, resulting from a decrease in state 3 and an increase of state 4 respirations. At this age, low ATP production by mitochondria isolated from 3xTg-AD mice (Table **2**) confirm that their ability to couple oxygen consumption to ADP phosphorylation during state 3 of respiration is compromised. Mitochondrial complexes I, II, and IV and F_oF_1-ATPase activities were evaluated and normalized with CS activity in order to discern between mitochondrial dysfunction and simple differences in the mitochondria content of the preparations used to assess the enzymes activities [44]. Additionally, CS normalized data also show a correlation between enzymatic activities and the morphometric characteristic of mitochondria in skeletal muscle tissue [44]. Fig. (**3**) displays the skeletal muscle mitochondrial complexes activities of nonTg and 3xTg-AD mice with 3, 6 and 12 months of age. Differences between nonTg and 3xTg-AD groups are only detected at 12 months of age with a significant decrease of complex I activity in 3xTg-AD mitochondria (nonTg 2.42±0.25, 3xTg-AD 1.44±0.29). Fig. (**3**) shows that aging is characterized by enzyme specific alterations. Complex I and complex IV activities tend to increase with age while complex II and F_oF_1-ATPase reach their maximum activity at 6 months of age.

Fatty Acids Profile of Skeletal Muscle Mitochondria

Fatty acids profile of skeletal muscle mitochondria obtained from 3xTg-AD and respective age-matched nonTg mice is displayed in Fig. (**4**) and the age-related changes in fatty acids profile are shown in Supplementary Fig. (**1**). At 3 months of age, mitochondria from 3xTg-AD mice exhibit higher monounsaturated fatty acids (MUFA) content, as a consequence of a significant increase in the relative abundance of oleic acid (C18:1). Additionally, at this age, the pathological condition is characterized by a significant decrease on the relative abundance of C18:0, C14:1, C20:4n-6 and C22:6n-3 in mitochondrial membranes (Fig. **4A**). The changes in the relative abundance of those fatty acids promote a decrease in the peroxidability and un-saturation indexes, which reflect a lower susceptibility to lipid peroxidation (Fig. **4D**). Curiously, at 6 months of age mitochondria from 3xTg-AD mice exhibit a fatty acids profile characterized by a significant recuperation of all fatty acids depressed at 3 months of age. Furthermore, the relative abundance of C20:4n-6 becomes significantly higher than in nonTg animals. On the other hand, mitochondria from 3xTg-AD mice are deficient in MUFA and n-3 polyunsaturated fatty acids (PUFA), resulting from decreased C16:1 and C18:3n-3 contents, respectively (Figs. **4B**, **4D**). At12 months of age, C16:1 and C22:6n-3 fatty acids are significant augmented in mitochondria from 3xTg-AD mice promoting an increase of n-3 PUFA and peroxidability index (Figs. **4C**, **4D**).

Phospholipid Profile of Skeletal Muscle Tissue from Mice with 12 Months-Old

In order to evaluate putative changes in the phospholipid profile of skeletal muscle tissue associated with Alzheimer`s disease, we used lipid extracts obtained from skeletal muscle homogenates from animals with 12 months of age, since it is only at this age that amyloid-β deposits and hyperphosphorylated tau, the histopathological hallmarks of the disease, are present in 3xTg-AD mice brains [32]. Separation of phospholipid classes was accomplished by HPLC-MS permitting the fractionation and identification of lyso-phosphatidylcholine (LPC), sphingomyelin (SM), phosphati

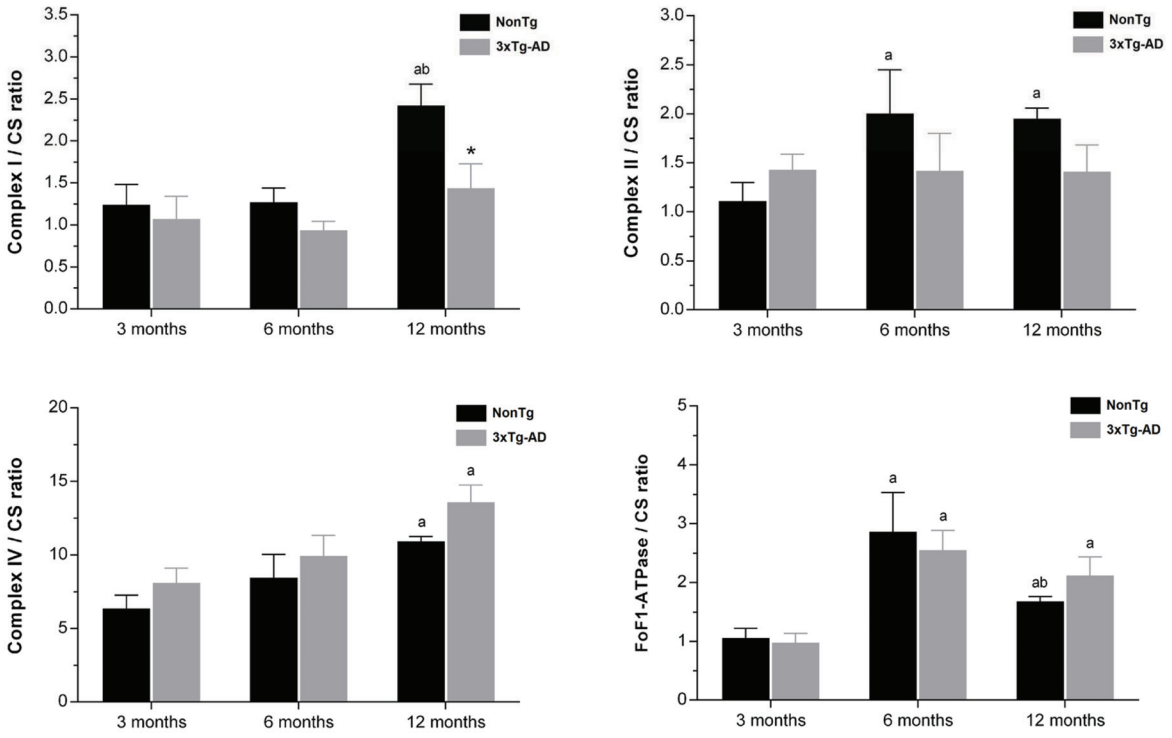

Fig. (3). Mitochondrial complexes I, II and IV and F_oF_1 ATPase activities normalized by citrate synthase activity (CS). Black and gray bars represent skeletal muscle mitochondria isolated from nonTg and 3xTg-AD mice, respectively, with 3, 6 and 12 months of age. Error bars represent standard deviation for n≥3 independent experiments using 3 animals in each one.* Significantly different from nonTg group, with p≤0.05. [a, b] Significantly different from 3 and 6 months of age, respectively, with p≤0.05.

dylcholine (PC), phosphatidylinositol (PI), phosphatidylserine (PS), phosphatidylethanolamine (PE), cardiolipin (CL). Each phospholipid specie was quantified determining the ratio of its peak area in MS-chromatogram to the respective internal standard and, its relative abundance in skeletal muscle tissue was determined after normalization by the total phosphorus amount in lipid extract. It is important to note that all species identified account for approximately 95% and 97% of the total phospholipids obtained in nonTg and 3xTg-AD samples, respectively. The relative abundance of each class of phospholipids in skeletal muscle membranes is shown in Fig. (**5**). In both nonTg and 3xTg-AD lipid extracts, the most abundant phospholipids are PC followed by PE, which together comprise about 62% and 55% of the total phospholipid content, respectively. Lipid class composition of skeletal muscle tissue clearly changes in Alzheimer`s disease by the specific replacement of one class by another. The relative abundance of LPC in skeletal muscle of 3xTg-AD mice increases 100% and this increase compensates the 12% decrease in PC. Since, the relative abundance of choline-containing phospholipids (LPC + PC + SM) is essentially preserved in 3xTg-AD mice (nonTg 56.2%, 3xTg-AD 55.1%), the higher LPC content suggests that phospholipases A_2 (PLA_2) activity is significantly enhanced in skeletal muscle of 3xTg-AD animals with an expected impact on lipid signaling processes .On the other hand, in skeletal muscle of 3xTg-AD mice, PE content is decreased by 12% while the anionic phospholipid PI is increased by 15% (Fig. **5**).

Lipid extracts of skeletal muscle tissue from nonTg and 3xTg-AD mice with 12 months of age were also analyzed by HPLC-MS/MS in both positive- and negative-ion modes. Typical positive-ion ESI mass spectra and the relative abundance of the most representative molecular species of LPC, SM and PC is shown in Fig. (**6**). Additionally, structural information of choline-containing lipids was obtained by analyzing the MS/MS fragmentation pattern of the detected *m/z* ions in order to identify the distribution of acyl chains for each one. Qualitative analysis show that lipid profile of choline-containing lipids of 3xTg-AD mice skeletal muscle is comparable to that of control animals since both groups exhibit the same individual species of PC, LPC and SM phospholipids. However, detailed quantitative analysis emphasizes that choline phospholipids metabolism is significantly affected by Alzheimer`s-like pathology. Relative abundance of LPC molecular specie with *m/z* at 496 (16:0), 518 (18:3), 520 (18:2), 522 (18:1), 524 (18:0), 542 (20:5), 546 (20:3), 548 (20:2) and 570 (22:5) are significantly higher in 3xTg-AD mice (Fig. **6C**). On the other hand, the relative abundance of PC molecular species at *m/z* 782.7 (36:4), 806.5 (38:6), 810.6 (38:4), 834.7 (40:6) and 872.8 (42:1) is significantly decreased while the relative abundance of the molecular species at *m/z* 854.5 (42:10), 878.5 (44:12), 868.5 (42:3), 870.5 (42:2), 874.6 (42:0) and 822.6 (40:5) are increased in 3xTg-AD mice compared with age-matched nonTg mice (Fig. **6D**). Our results also suggest that the loss of arachidonic acid (C20:4n-6) of specific PC molecular species is associated with the increased level of LPC species. For example, the enzymatic cleavage of arachidonic acid from PC ions at *m/z* 782 (16:0/20:4) and 806(18:2/20:4) generate

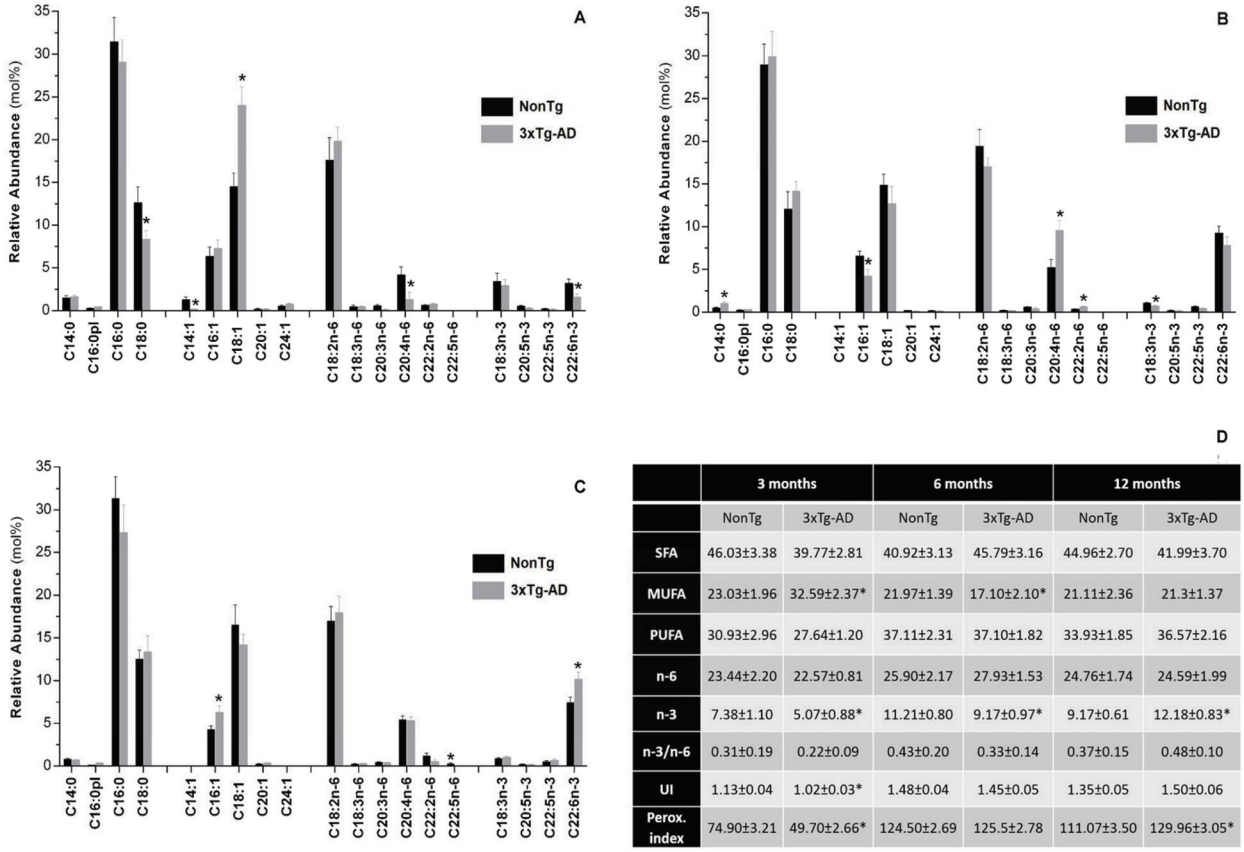

	3 months		6 months		12 months	
	NonTg	3xTg-AD	NonTg	3xTg-AD	NonTg	3xTg-AD
SFA	46.03±3.38	39.77±2.81	40.92±3.13	45.79±3.16	44.96±2.70	41.99±3.70
MUFA	23.03±1.96	32.59±2.37*	21.97±1.39	17.10±2.10*	21.11±2.36	21.3±1.37
PUFA	30.93±2.96	27.64±1.20	37.11±2.31	37.10±1.82	33.93±1.85	36.57±2.16
n-6	23.44±2.20	22.57±0.81	25.90±2.17	27.93±1.53	24.76±1.74	24.59±1.99
n-3	7.38±1.10	5.07±0.88*	11.21±0.80	9.17±0.97*	9.17±0.61	12.18±0.83*
n-3/n-6	0.31±0.19	0.22±0.09	0.43±0.20	0.33±0.14	0.37±0.15	0.48±0.10
UI	1.13±0.04	1.02±0.03*	1.48±0.04	1.45±0.05	1.35±0.05	1.50±0.06
Perox. index	74.90±3.21	49.70±2.66*	124.50±2.69	125.5±2.78	111.07±3.50	129.96±3.05*

Fig. (4). Fatty acid profile of total lipid extract obtained from skeletal muscle mitochondria isolated from nonTg (black bars) and 3xTg-AD (gray bars) mice with 3 (**A**), 6 (**B**) and 12 (**C**) months of age. C14:0 - myristic acid, C16:0pl - hexadecyl dimethyl acetal, C16:0 - palmitic acid, C18:0 - stearic acid, C14:1 - myristoleic acid, C16:1 - palmitoleic acid, C18:1 - oleic acid, C20:1 - eicosenoic acid, C24:1 - nervonic acid, C18:2n-6 - linoleic acid, C18:3n-6 - γ-linolenic acid, C20:3n-6 - dihomo-gamma-linolenic acid (DGLA), C20:4n-6 - arachidonic acid, C22:2n-6 - decosadienoic acid, C22:5n-6 - docosapentaenoic acid, C18:3n-3 - α-linolenic acid, C20:5n-3 - eicosapentaenoic acid (EPA), C22:5n-3 - docosapentaenoic acid n-3, C22:6n-3 - docosahexanoic acid (DHA). Table (**D**): general parameters of total lipid extract. SFA, saturated fatty acids; MUFA, monounsaturated fatty acids; PUFA, polyunsaturated fatty acids; UI, unsaturation index; Perox index, peroxidability index.*Significant difference between nonTg and 3xTg-AD groups, with $p \leq 0.05$.

LPC ions at *m/z* 496 (16:0/0:0) and 520 (18:2/0:0), respectively (Fig. **6**, Supplementary Table **2**).

Individual molecular species within PI, PS, PE and CL phospholipid classes from nonTg and 3xTg-AD mice skeletal muscle were analyzed in negative ionization mode and typical negative-ion ESI mass spectra are depicted in Figs. (**7A** and **8A**). PI molecular profile of nonTg and 3xTg-AD mice consists of 3 different species with corresponding *m/z* at 885.6 (38:4), 887.8 (38:3) and 909.6 (40:6) (Supplementary Table **3**). Even though molecular species diversity and fatty acids distribution within individual molecular species are similar between experimental groups, quantitative analysis reveals that the relative abundance of PI molecular species at *m/z* 885.6 (38:4) and 909.6 (40:6) are respectively increased and decreased in 3xTg-AD mice (Fig. **7B**). Likewise, HPLC-MS/MS analysis in negative-ion mode shows that quantitative distribution of individual molecular species within PS, PE and CL phospholipid classes is altered in 3xTg-AD mice when compared with nonTg mice. PS profile exhibits significant changes in the relative abundance of molecular diacyl-PS species at *m/z* 844.5 (40:1), 864.5 (42:5) and 892.5 (44:5) and plasmalogens species at *m/z* 792.7 (o38:6) (Fig. **7C**, Supplementary Table **3**). In turn, alterations of PE molecular profile in 3xTg-AD group are detected by a decay in the relative abundance of diacyl-PE specie at *m/z* 770.5(38:2) and 788.6 (40:7) and plasmalogens species at *m/z* 772.5 (p40:7), 774.8 (p40:6), 776.5 (p40:5) and 784.8 o40:2) along with an increased relative abundance of molecular ion at *m/z* 790.8 (40:6) (Fig. **7D**, Supplementary Table **3**). CL profile of skeletal muscle from nonTg and 3xTg-AD mice with 12 months of age is shown in Fig. (**8**). Single charge $[M-H]^-$ MS spectra shows that CL profile of skeletal muscle from nonTg and 3xTg-AD mice is represented by three major clusters (Fig. **8A**). Even though the relative abundance of CL is similar in both experimental groups (Fig. **5**), quantitative analysis revealed alterations in individual CL molecular species distribution (Fig. **8B**). Particularly, $[M-H]^-$ ions at *m/z* 1379.8 (66:0); 1479.8 (74:6); 1551.9 (80:6); 1569.9 (80:3) and 1577.8 (82:13) are increased in 3xTg-AD mice while molecular ions at *m/z* 1501.8 (76:9); 1525.9 (78:11); 1555.8 (80:10); 1579.8 (82:12); 1581.8 (82:11) are decreased in these animals (Fig. **8B**). Despite alterations in the quantitative distribution of individual molecular species within the CL class, pathological situation does not affect species diversity neither the fatty acids distribution within each molecular specie (Supplementary Table **4**).

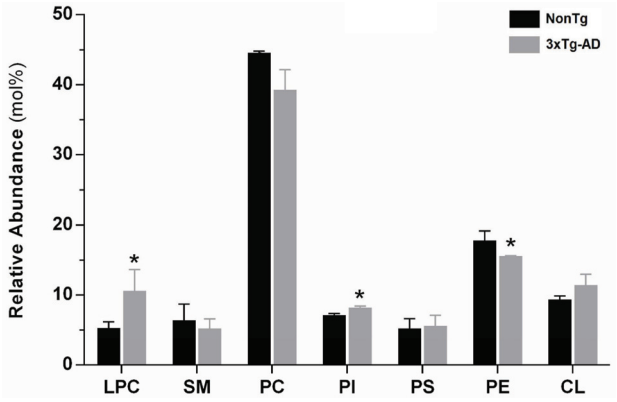

Fig. (5). Relative abundance (mol%) of each phospholipid classes in total lipid extract of skeletal muscle tissue from nonTg (black bars) and 3xTg-AD (gray bars) mice with 12 months of age. LPC, lysophosphatidylcholine, SM, sphingomyelin, PC, phosphatidylcholine, PI, phosphatidylinositol, PS, phosphatidylserine, PE, phosphatidylethanolamine, CL, cardiolipin. Error bars represent standard deviation for n=3 independent experiments using 3 animals each in each one. The amount of each phospholipid class was calculated by the sum of its individual species identified and quantified by HPLC-MS/MS, as described in methods section. Considering the results as total nmoles of phospholipids per mg of protein in skeletal muscle homogenates: nonTg 107.66±18.30 and 3xTg-AD 90.32±10.20. * Significantly different from nonTg group, with $p \leq 0.05$.

DISCUSSION

Alzheimer`s disease brain pathology is characterized by deposits of amyloid-β peptides and neurofibrillary tangles and by other metabolic alterations that include the disruption of redox balance, bioenergetics and lipid metabolism abnormalities and chronic inflammation [6-8, 45]. Additionally, some of those changes including the anomalous APP proteolytic processing and amyloid-β peptide accumulation are not restrict to brain since they are also detected in peripheral tissues (e.g. skeletal muscle) of both Alzheimer's human subjects and animal models of the disease [3, 46, 47]. In this way, Alzheimer`s pathology can be considered a systemic disease and the characterization of the phenotype related to peripheral tissues offers the opportunity to identify new biomarkers that may facilitate the early diagnosis of Alzheimer`s disease [48]. In the present work, 3xTg-AD mice were used as animal model of Alzheimer`s disease since they have three gene mutations, namely APP_{Swe}, $PS1_{M146V}$, and tau_{P301L}, which cause the development of the pathological hallmarks of the disease in an age-dependent manner [32, 49]. As previously described, mice with 3 months of age are considered to be in a pre-symptomatic stage, at 6 months of age extracellular amyloid-β deposits are detected predominantly in the frontal cortex and, at 12 months of age, both amyloid-beta and tau pathologies are detected [28, 32]. Thus, to evaluate

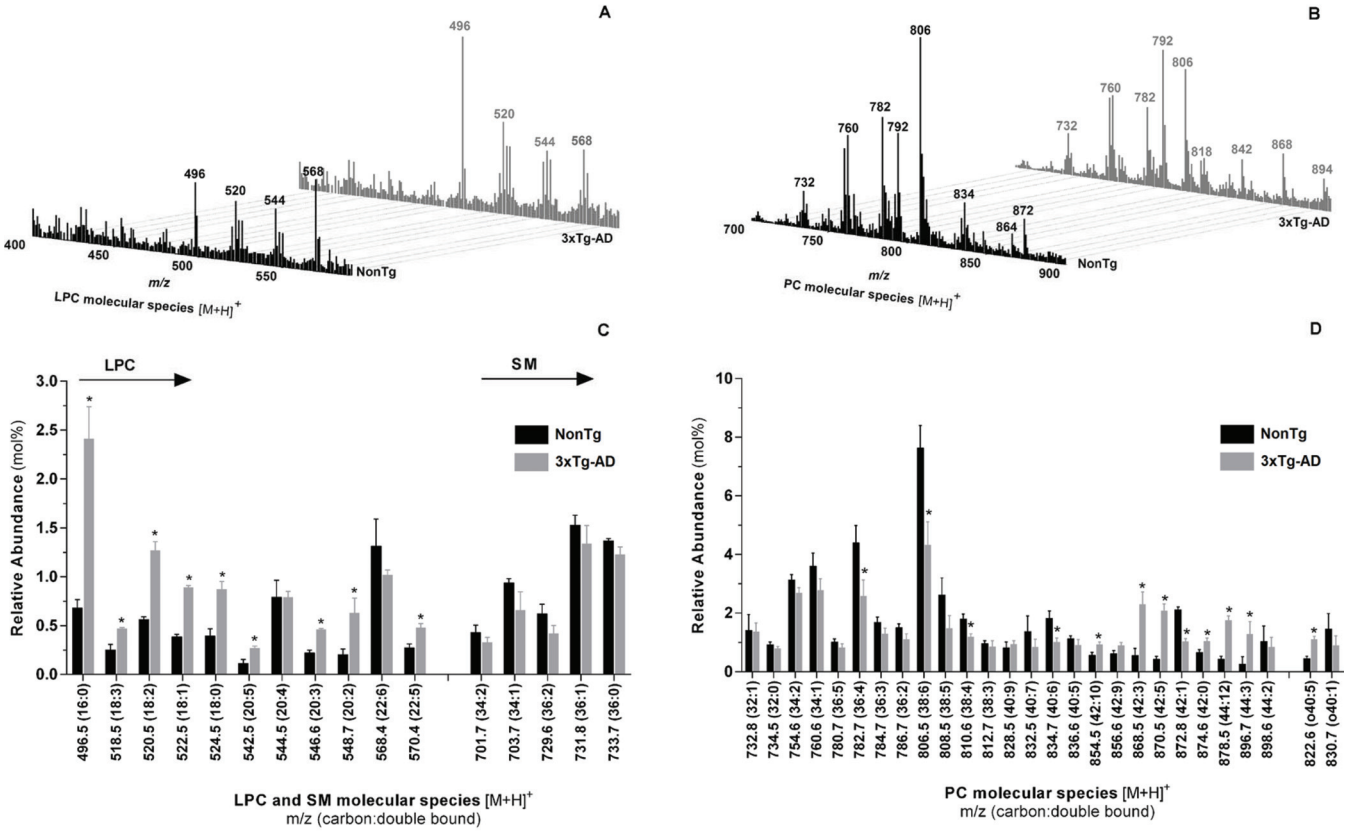

Fig. (6). Molecular profile of choline lipids extracted from skeletal muscle homogenates of nonTg (black bars) and 3xTg-AD (gray bars) mice with 12 months of age. Typical ESI-MS in positive mode with formation of $[M+H]^+$ ions of PC, LPC and SM (**A, B**). Distribution of LPC (**C**), SM (**C**) and PC (**D**) molecular species. Error bars represent standard deviation for n=3 independent experiments using 3 animals in each one. * Significantly different from nonTg group, with $p \leq 0.05$

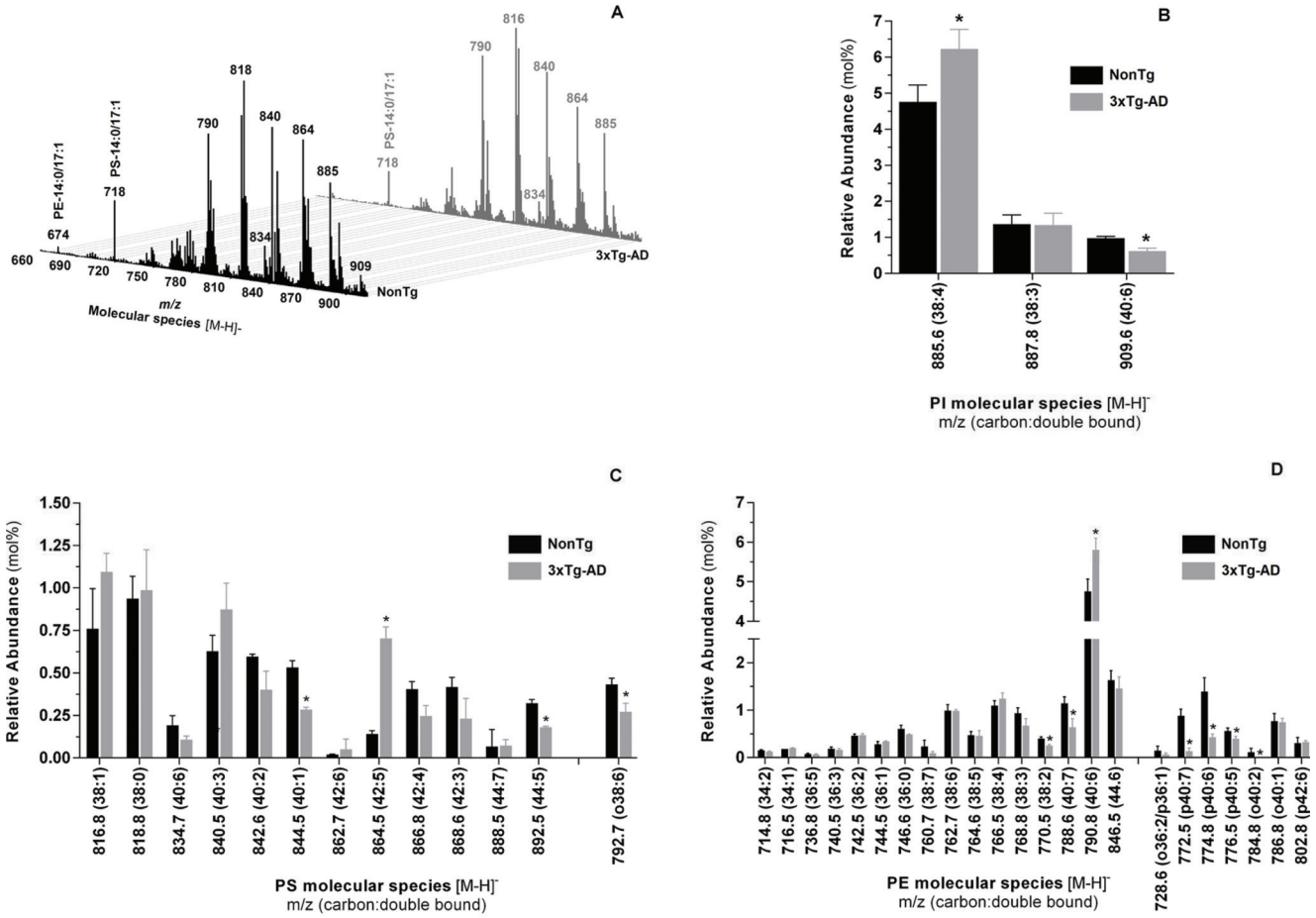

Fig. (7). Molecular profile of PI, PS and PE extracted from skeletal muscle homogenates of nonTg (black bars) and 3xTg-AD (gray bars) mice with 12 months of age. Typical ESI-MS obtained in negative ion mode (**A**) and the respective distribution of PI (**B**), PS (**C**) and PE (**D**) molecular species. Error bars represent standard deviation for n=3 independent experiments using 3 animals in each one. * Significantly different from nonTg group, with $p \leq 0.05$.

the biochemical skeletal muscle changes during the evolution of Alzheimer`s disease we performed studies in animals with 3, 6 and 12 months of age.

Our results showed that regulation of skeletal muscle activity by acetylcholine may be compromised in 3xTg-AD mice, since a decrease in maximal AChE activity was early and consistently detected during disease progression (Fig. **1**). These results suggest a down-regulation of AChE in 3xTg-AD mice, which can emerge from a compensatory mechanism in response to a defective acetylcholine release from cholinergic neurons in the neuromuscular junction or from morphological and functional changes in neuromuscular synapses related with mutations in the APP gene, as previously described [50-52]. Since AChE is a membrane bound enzyme, changes in the biophysical properties of plasma membranes of skeletal muscle cells may also contribute to the decrease of its maximal activity.

Regarding the enzymatic antioxidant defenses of skeletal muscle, our results revealed that 3xTg-AD mice have a significant low catalase activity than age-matched controls while no differences were found for SOD activity (Fig. **2**). Therefore, skeletal muscle of 3xTg-AD mice has a lower ability to prevent oxidative stress induced by H_2O_2-derived hydroxyl radicals. In agreement, significant reductions in catalase activity and unchanged SOD activity have been also observed in postmortem human Alzheimer`s disease brains [53]. The evident accumulation of amyloid-β peptides in skeletal muscle of 3xTg-AD mice with 6 and 12 months of age (Table **1**) may also contribute to the decrease of catalase activity, since *in vitro* studies have demonstrate that soluble and/or oligomeric forms of amyloid-β peptides interact with catalase decreasing its activity [54]. Until 12 months of age, skeletal muscle of 3xTg-AD mice did not show changes in the redox status of cellular thiols, which *in vivo* are mainly oxidized by peroxides (e.g. peroxynitrite anion, superoxide) and regulated by an enzymatic system that include glutathione reductase and glutathione peroxidase [55].

The bioenergetics analyses revealed that 3xTg-AD mice with 3 and 6 months of age exhibit functional skeletal muscle mitochondria since no significant changes were detected in both RCR and ADP/O indexes (Table **2**) nor in the individual activity of key enzymatic complexes linked with oxidative phosphorylation, namely mitochondrial complexes I, II, IV and F_oF_1-ATPase (Fig. **3**). However, mitochondrial deficits in skeletal muscle of 3xTg-AD mice became apparent at 12 months of age by a significant decrease of RCR and ADP/O index associated with a decay in complex I activity.

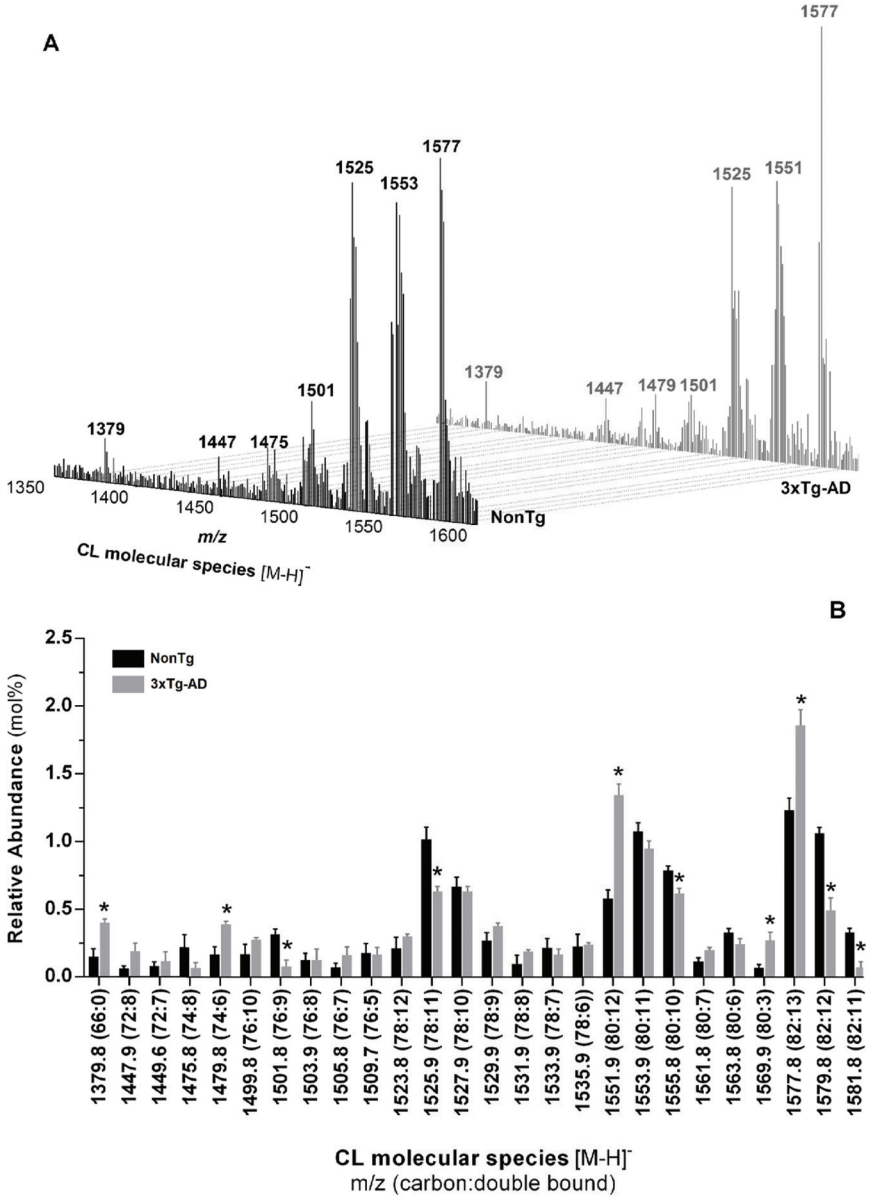

Fig. (8). Molecular profile of CL extracted from skeletal muscle homogenates of nonTg (black bars) and 3xTg-AD (gray bars) mice with 12 months of age. Typical ESI-MS of CL obtained in negative ion mode (**A**) and the respective distribution molecular species (**B**). Error bars represent standard deviation for n=3 independent experiments using 3 animals in each one. *Significantly different from non Tg group, with $p \leq 0.05$.

In opposition to what occurs in brain, where synaptic mitochondria dysfunction is already detected at 3 months of age [7, 43, 56], our observations suggest that the increase in amyloid-β peptide levels in skeletal muscle of 3xTg-AD mice may precede and contribute to skeletal muscle mitochondrial dysfunction. Substantial alterations in mitochondrial structure and function associated with increased levels of amyloid-βin skeletal muscle have been also described in MCK-β APP transgenic mice [9]. Another study has shown a decrease in mitochondrial p-trifluoromethoxyphenylhydrazone-uncoupled respiration in single fibers isolated from APP_{Swe}/ $PS1_{\Delta E9}$ double transgenic mice with 3 months of age. In this Alzheimer's disease mouse model mitochondrial bioenergetics dysfunction occurs simultaneously in both brain and skeletal muscle tissues, these alterations preceding the presence of senile plaques in brain [57]. However, skeletal muscle is a spatial regionalized metabolic tissue that exhibit various fiber types, each one with a dynamic mitochondrial network system containing different populations of mitochondria (*e.g.* subsarcolemmal, perinuclear, interfibrillar) with specific functional morphology largely determined by fusion and fission processes [58]. Thus, the bioenergetics deficit detected in mitochondria isolated from muscles removed from intercostal and legs body regions of 3xTg-AD mice with 12 months, is not necessarily an homogenous effect occurring on all fiber types since it can also emerge from changes in a specific mitochondria population in just one type of fibers reflecting problems in the dynamic mitochondrial network system in skeletal muscle tissue.

Since lipid composition of mitochondrial membranes modulates the activity of their host enzymes and reflects the general metabolic state of the cell, fatty acids profile of skeletal muscle mitochondria were evaluated in nonTg and 3xTg-AD mice in order to detect changes in lipid metabolism putatively connected with aging and Alzheimer`s disease progression. In healthy animals, aging has a strong impact on the composition of n-3 PUFA characterized by a decrease of short chain fatty acids, C18:3n-3 and C20:5n-3, and an increase of 22 carbons long chain fatty acids, C22:5n-3 and C22:6n-3 (Supplementary Fig. **1**). These alterations, particularly marked between 3 and 6 months, cause an increase in unsaturation and peroxidability indexes (Fig. **4**) with at least two functional consequences i) increased capacity of mitochondrial ATP production, as detected in this work (Table **2**) and by others [59], and ii) increased mitochondrial membranes propensity for oxidative processes. The increased activity of antioxidant enzymes SOD and catalase, between 3 and 6 months of age (Fig. **2**), may emerge as a balancing mechanism to avoid the oxidative damage. In 3xTg-AD animals, aging leads to similar n-3 PUFA content changes with increased unsaturation index required to improve the capacity to oxidative energy production (Table **2**). However, 3xTg-AD animals appears to be more susceptible to oxidative damage since they are less effective triggering an adaptive response as indicated by low catalase activity (Fig. **2**). Unlike nonTg mice, 3xTg-AD mice are also unable to keep stable the mitochondrial membrane content of C18:0, C18:1 and C20:4n-6 during aging process, suggesting that the lack of lipid metabolism control is associated with Alzheimer's-like pathology developed by those animal. In this way, dysregulation of mitochondrial lipid metabolism in skeletal muscle of 3xTg-AD mice precedes the bioenergetics deficits which may results from oxidative damage and/or mitochondrial toxicity of amyloid-β peptide [60]. Alteration of lipid metabolism was early identified by Dr. Alois Alzheimer as a characteristic of brains suffering from Alzheimer's disease [61]. Currently, it is known that the biophysical properties and dynamic organization of biomembranes can be modulated through molecular mechanisms associated with Alzheimer's disease. Specifically, amyloid-β peptide can interact with cellular membranes impairing their integrity and leading to changes in membrane-dependent signaling pathways. Additionally, dysregulated calcium homeostasis, strictly connected with neurofibrillary tangles formation, can also interfere with phospholipid-metabolizing enzymes (e.g. phospholipases, lipoxygenases) and thus impact on membrane organization and lipid signaling [62]. Thus, we examined the lipidome of skeletal muscle of 12-month-old nonTg and 3xTg-AD mice since at this age, transgenic animals, in addition to the brain hallmarks (amyloid-beta and tau pathologies) of the disease, exhibit alterations in skeletal muscle mitochondrial bioenergetics and increased amyloid-β levels.

HPCL-MS/MS analysis revealed that increased LPC levels in skeletal muscle tissue of 3xTg-AD animals results from a decay of specific PC molecular species from which arachidonic acid was enzymatically removed. Previously, it was shown that cytoplasmic calcium-depend PLA_2 ($cPLA_2$) preferentially cleaves arachidonic acid from *sn-2* position of PC [63]. Thus, our data suggest that $cPLA_2$ is up-regulated in skeletal muscle of 3xTg-AD mice. Similarly, increased LPC levels and $cPLA_2$ activity, were observed in the cerebrospinal fluid of Alzheimer's patients [64]. Increased levels of LPC can perturb membrane biophysical organization [65] interfering with non-amyloidogenic processing of APP with consequent production of amyloid-β peptides well evidenced by the increased amyloid-β_{1-40} levels detected in 3xTg-AD mice (Table **1**). LPC itself can also activate G protein coupled receptors such as G2A, which is involved in immune cellular responses [66]. In p25Tg mice brain, LPC acts as a molecular signal that mediate glial activation and the recruitment of inflammatory mediators contributing to Alzheimer's-like pathology [67]. Furthermore, free arachidonic acid and its oxidized active metabolites (*e.g.* prostaglandins, thromboxanes and leukotrienes), which play key roles in the inflammatory processes, have been also associated with Alzheimer`s disease [62]. Amtul and coworkers (2012) combining *in vitro* and *in vivo* studies showed that arachidonic acid and its pro-inflammatory metabolites are involved in the overproduction of amyloid-β_{1-40} and amyloid-β_{1-42} and Alzheimer's pathogenesis [68]. In agreement, our results in skeletal muscle support the idea that amyloid-β overproduction and arachidonic acid released from PC molecular species with consequent increase of LPC levels are interconnected events contributing to skeletal muscle dysfunction in 3xTg-AD mice.

Consistent with other studies made in brain [69], cerebrospinal fluid [64] and serum [70], skeletal muscle of 3xTg-AD mice presented a significant decrease of PE levels (Fig. **5**) mainly associated with alterations in PE-plasmalogens species (Fig. **7**). It was proposed that brain PE-plasmalogens deficiency promotes cell membrane instability and link neurodegeneration to cholinergic system dysfunction in Alzheimer`s brain [69]. Thus, PE-plasmalogens deficiency may have functional consequences on skeletal muscle of 3xTg-AD mice. Lipid metabolism dysregulation in skeletal muscle of 3xTg-AD is also evidenced by minor changes in the profile of anionic phospholipid classes (PS, PI and CL). For example, overall PI content increase in skeletal muscle of 3xTg-AD mice and n-3/ n-6 PUFA ratio decreased as a consequence of alterations in the levels of molecular species at *m/z* 909.5 (18:0/22:6) and 885.6 (18:0/20:4), which are respectively decreased and increased (Fig. **7**, Supplementary Table **3**). On the other hand, changes in MS profile of CL of 3xTg-AD mice muscle tissue in relation to age-matched controls (Fig. **8**) reflect mitochondria-specific changes in lipid metabolism, which was also apparent by GC-MS analyses of mitochondrial lipids (Fig. **4**). These alterations may be connected with the bioenergetics deficit and the increased amyloid-β levels in skeletal muscle tissue of 3xTg-AD mice with12 months of age (Fig. **3**, Tables **1, 2**).

CONCLUSION

Summarizing the data presented in this study it can be concluded that Alzheimer`s-like pathology progressively developed by 3xTg-AD mice is not exclusive to brain tissue since several pathologic signs correlated with brain pathology are also detected in skeletal muscle. Deficient AChE and catalase activities were detected in skeletal muscle of 3xTg-AD mice at 3 months of age, prior to brain amyloid-β deposits indicating early changes in skeletal

muscle associated with Alzheimer`s-like pathology. Similarly to the brain, increased levels of amyloid-β_{1-40} in skeletal muscle of 3xTg-AD mice is an age-dependent process suggesting that APP amyloidogenic processing is a systemic issue in Alzheimer's disease biology. Additionally, the increased levels of amyloid-β peptides in the skeletal muscle of 3xTg-AD mice precedes and may contribute to mitochondrial dysfunction, which is only detected at 12 months of age and characterized by decreased RCR and ADP/O ratio and impaired complex I activity. Lipidomic studies suggest that the molecular mechanisms used by cells to dynamically adjust the lipid composition of their membranes are dysregulated in skeletal muscle of 3xTg-AD mice. Firstly, the age-related evolution of the mitochondrial fatty acids profile in skeletal muscle tissues of 3xTg-AD mice shows significant differences as compared to nonTg animals, which are particularly apparent at 3 months of age, preceding the increase in amyloid-β peptide levels and bioenergetics deficit. Secondly, at 12 months of age skeletal muscle tissue of 3xTg-AD mice exhibits a prevalent unbalance of phospholipid metabolism, which was detected by a significant decrease in PC and PE-plasmalogens and by an increase in LPC and PI levels. The alterations in phospholipid composition of cell membranes can compromise their dynamic organization and impair the correct functioning of the embedded membrane proteins triggering anomalous cellular processes, including the abnormal APP metabolism promoting the increase in the levels of amyloid-β peptides. Additionally, the increased levels of LPC are immediately linked with a decrease of PC molecular species containing arachidonic acid indicating an enhanced $cPLA_2$ activity as well as increased inflammation in skeletal muscle of 3xTg-AD mice. The decrease of PE-plasmalogens associated with a decrease in catalase activity also suggest a decreased antioxidant capacity in skeletal muscle of 3xTg-AD mice compared with nonTg mice. The present study shows that in 3xTg-AD mice, a relevant animal model for Alzheimer`s disease, a great parallelism exists between the pathophysiological changes occurring in brain and skeletal muscle tissues. These observations support the idea that skeletal muscle biochemical alterations can be used as potential diagnostic biomarker of Alzheimer`s disease and follow up of changes associated with disease progression.

ABBREVIATIONS

AChE = Acetylcholinesterase

APP = Amyloid precursor protein

CL = Cardiolipin

DCPIP = 6,6-dichlorophenolindophenol

DTNB = 5,5'-dithiobis (2-nitrobenzoic acid

FAME = Fatty acid methyl ester

LPC = Lyso-phosphatidylcholine

MUFA = Monounsaturated fatty acids

NBT = Nitro blue tetrazolium

PC = Phosphatidylcholine

PE = Phosphatidylethanolamine

PI = Phosphatidylinositol

PLA_2 = Phospholipase A_2

PS = Phosphatidylserine

PUFA = Polyunsaturated fatty acids

RCR = Respiratory control ratio

SM = Sphingomyelin

SOD = Superoxide dismutase

TLC = Thin layer chromatography

TMPD = *N*,*N*,*N*',*N*'-tetramethyl-1,4-benzenediamine dihydrochloride

TNB = 5-thio-2-nitrobenzoic acid

CONFLICT OF INTEREST

The authors confirm that this article content has no conflict of interest.

ACKNOWLEDGEMENTS

This work was supported by Foundation for Science and Technology (FCT), and European Union Funds (FEDER/COMPETE) [Project Grants: PTDC/SAU NMC/115865/2009; PEst-OE/QUI/UI0616/2014]. Vera F. Monteiro-Cardoso is supported by FCT grant BI/PTDC/SAU-NMC/115865/2009.

SUPPLEMENTARY MATERIALS

Supplementary material is available on the publishers web site along with the published article.

REFERENCES

[1] Serrano-Pozo A, Frosch MP, Masliah E, Hyman BT. Neuropathological alterations in Alzheimer disease. Cold Spring Harb Perspect Med 1(1): a006189 (2011).

[2] Arai Y, Suzuki A, Mizuguchi M, Takashima S. Developmental and aging changes in the expression of amyloid precursor protein in Down syndrome brains. Brain Dev-Jpn 19(4): 290-4 (1997).

[3] Kuo YM, Crawford F, Mullan M, Kokjohn TA, Emmerling MR, Weller RO*, et al.* Elevated A beta and apolipoprotein E in A beta PP transgenic mice and its relationship to amyloid accumulation in Alzheimer's disease. Mol Med 6(5): 430-9 (2000).

[4] Burns JM, Johnson DK, Watts A, Swerdlow RH, Brooks WM. Reduced Lean Mass in Early Alzheimer Disease and Its Association With Brain Atrophy. Arch Neurol-Chicago 67(4): 428-33 (2010).

[5] Mckhann G, Drachman D, Folstein M, Katzman R, Price D, Stadlan EM. Clinical-Diagnosis of Alzheimers-Disease - Report of the Nincds-Adrda Work Group under the Auspices of Department-of-Health-and-Human-Services Task-Force on Alzheimers-Disease. Neurology 34(7): 939-44 (1984).

[6] Ding F, Yao J, Rettberg JR, Chen S, Brinton RD. Early decline in glucose transport and metabolism precedes shift to ketogenic system in female aging and Alzheimer's mouse brain: implication for bioenergetic intervention. PloS one 8(11): e79977 (2013).

[7] Du H, Guo L, Yan S, Sosunov AA, McKhann GM, Yan SS. Early deficits in synaptic mitochondria in an Alzheimer's disease mouse model. Proc Natl Acad Sci USA 107(43): 18670-5 (2010).

[8] Hauptmann S, Scherping I, Drose S, Brandt U, Schulz KL, Jendrach M*, et al*. Mitochondrial dysfunction: an early event in Alzheimer pathology accumulates with age in AD transgenic mice. Neurobiol Aging 30(10): 1574-86 (2009).

[9] Boncompagni S, Moussa CEH, Levy E, Pezone MJ, Lopez JR, Protasi F*, et al.* Mitochondrial Dysfunction in Skeletal Muscle of

Amyloid Precursor Protein-overexpressing Mice. J Biol Chem 287(24): 20534-44 (2012).
[10] Iyo M, Namba H, Fukushi K, Shinotoh H, Nagatsuka S, Suhara T, *et al.* Measurement of acetylcholinesterase by positron emission tomography in the brains of healthy controls and patients with Alzheimer's disease. Lancet 349(9068): 1805-9 (1997).
[11] Teipel SJ, Flatz WH, Heinsen H, Bokde ALW, Schoenberg SO, Stockel S, *et al.* Measurement of basal forebrain atrophy in Alzheimer's disease using MRI. Brain 128: 2626-44 (2005).
[12] Herholz K, Carter SF, Jones M. Positron emission tomography imaging in dementia. Brit J Radiol 80: S160-S7 (2007).
[13] Hanyu H, Asano T, Sakurai H, Tanaka Y, Takasaki M, Abe K. MR analysis of the substantia innominata in normal aging, Alzheimer disease, and other types of dementia. Am J Neuroradiol 23(1): 27-32 (2002).
[14] Davis KL, Mohs RC, Marin D, Purohit DP, Perl DP, Lantz M, *et al.* Cholinergic markers in elderly patients with early signs of Alzheimer disease. JAMA 281(15): 1401-6 (1999).
[15] Davies P, Maloney AJF. Selective Loss of Central Cholinergic Neurons in Alzheimers-Disease. Lancet 2(8000): 1403- (1976).
[16] Perry EK, Perry RH, Blessed G, Tomlinson BE. Necropsy Evidence of Central Cholinergic Deficits in Senile Dementia. Lancet 1(8004): 189- (1977).
[17] Liston DR, Nielsen JA, Villalobos A, Chapin D, Jones SB, Hubbard ST, *et al.* Pharmacology of selective acetylcholinesterase inhibitors: implications for use in Alzheimer's disease. Eur J Pharmacol 486(1): 9-17 (2004).
[18] Kaduszkiewicz H, Zimmermann T, Beck-Bornholdt HP, van den Bussche H. Cholinesterase inhibitors for patients with Alzheimer's disease: systematic review of randomised clinical trials. Brit Med J 331(7512): 321-3 (2005).
[19] Melo T, Videira RA, Andre S, Maciel E, Francisco CS, Oliveira-Campos AM, *et al.*Tacrine and its analogues impair mitochondrial function and bioenergetics: a lipidomic analysis in rat brain. J Neurochem 120(6): 998-1013 (2012).
[20] Mesulam M. The cholinergic lesion of Alzheimer's disease: Pivotal factor or side show? Learn Memory 11(1): 43-9 (2004).
[21] Massoulie J. The origin of the molecular diversity and functional anchoring of cholinesterases. Neurosignals 11(3): 130-43 (2002).
[22] Fishman EB, Siek GC, MacCallum RD, Bird ED, Volicer L, Marquis JK. Distribution of the molecular forms of acetylcholinesterase in human brain: alterations in dementia of the Alzheimer type. Ann Neurol 19(3): 246-52 (1986).
[23] Saez-Valero J, Sberna G, McLean CA, Small DH. Molecular isoform distribution and glycosylation of acetylcholinesterase are altered in brain and cerebrospinal fluid of patients with Alzheimer's disease. J Neurochem 72(4): 1600-8 (1999).
[24] Saez-Valero J, de Ceballos ML, Small DH, de Felipe C. Changes in molecular isoform distribution of acetylcholinesterase in rat cortex and cerebrospinal fluid after intracerebroventricular administration of amyloid beta-peptide. Neurosci Lett 325(3): 199-202 (2002).
[25] Garcia-Ayllon MS, Small DH, Avila J, Saez-Valero J. Revisiting the Role of Acetylcholinesterase in Alzheimer's Disease: Cross-Talk with P-tau and beta-Amyloid. Front Mol Neurosci 4: 22 (2011).
[26] Silveyra MX, Garcia-Ayllon MS, de Barreda EG, Small DH, Martinez S, Avila J, *et al.* Altered expression of brain acetylcholinesterase in FTDP-17 human tau transgenic mice. Neurobiol Aging 33(3): 624 e23-34 (2012).
[27] Talesa VN. Acetylcholinesterase in Alzheimer's disease. Mech Ageing Dev 122(16): 1961-9 (2001).
[28] Gimenez-Llort L, Blazquez G, Canete T, Johansson B, Oddo S, Tobena A, *et al.* Modeling behavioral and neuronal symptoms of Alzheimer's disease in mice: a role for intraneuronal amyloid. Neurosci Biobehav Rev 31(1): 125-47 (2007).
[29] Coleman BA, Taylor P. Regulation of acetylcholinesterase expression during neuronal differentiation. J Biol Chem 271(8): 4410-6 (1996).
[30] Chan RB, Oliveira TG, Cortes EP, Honig LS, Duff KE, Small SA, *et al.* Comparative lipidomic analysis of mouse and human brain with Alzheimer disease. J Biol Chem 287(4): 2678-88 (2012).
[31] Di Paolo G, Kim TW. Linking lipids to Alzheimer's disease: cholesterol and beyond. Nature reviews Neurosci 12(5): 284-96 (2011).
[32] Oddo S, Caccamo A, Kitazawa M, Tseng BP, LaFerla FM. Amyloid deposition precedes tangle formation in a triple transgenic model of Alzheimer's disease. Neurobiol Aging 24(8): 1063-70 (2003).
[33] Gornall AG, Bardawill CJ, David MM. Determination of serum proteins by means of the biuret reaction. J Biol Chem 177(2): 751-66 (1949).
[34] Spitz DR, Oberley LW. An assay for superoxide dismutase activity in mammalian tissue homogenates. Anal Biochem 179(1): 8-18 (1989).
[35] Del Rio LA, Ortega MG, Lopez AL, Gorge JL. A more sensitive modification of the catalase assay with the Clark oxygen electrode. Application to the kinetic study of the pea leaf enzyme. Anal Biochem 80(2): 409-15 (1977).
[36] Hu ML. Measurement of protein thiol groups and glutathione in plasma. Methods Enzymol 233: 380-5 (1994).
[37] Skalska J, Piwonska M, Wyroba E, Surmacz L, Wieczorek R, Koszela-Piotrowska I, *et al.*A novel potassium channel in skeletal muscle mitochondria. Biochimica et biophysica acta 1777(7-8): 651-9 (2008).
[38] Cardoso S, Santos RX, Correia SC, Carvalho C, Santos MS, Baldeiras I, *et al.* Insulin-induced recurrent hypoglycemia exacerbates diabetic brain mitochondrial dysfunction and oxidative imbalance. Neurobiol Dis 49C: 1-12 (2012).
[39] Monteiro-Cardoso VF, Silva AM, Oliveira MM, Peixoto F, Videira RA. Membrane lipid profile alterations are associated with the metabolic adaptation of the Caco-2 cells to aglycemic nutritional condition. J Bioenerg Biomembr 46(1): 45-57 (2014).
[40] Bartlett GR. Phosphorus Assay in Column Chromatography. J Biol Chem 234(3): 466-8 (1959).
[41] Peixoto F, Vicente J, Madeira VMC. A comparative study of plant and animal mitochondria exposed to paraquat reveals that hydrogen peroxide is not related to the observed toxicity. Toxicol *in vitro* 18(6): 733-9 (2004).
[42] Kuo YM, Kokjohn TA, Watson MD, Woods AS, Cotter RJ, Sue LI, *et al.* Elevated abeta42 in skeletal muscle of Alzheimer disease patients suggests peripheral alterations of AbetaPP metabolism. Am J Pathol 156(3): 797-805 (2000).
[43] Monteiro-Cardoso VF, Oliveira MM, Melo T, Domingues MR, Moreira PI, Ferreiro E, *et al.*Cardiolipin Profile Changes are Associated to the Early Synaptic Mitochondrial Dysfunction in Alzheimer's Disease. J Alzheimers Dis 43(4): 1375-92 (2015).
[44] Gellerich FN, Deschauer M, Chen Y, Muller T, Neudecker S, Zierz S. Mitochondrial respiratory rates and activities of respiratory chain complexes correlate linearly with heteroplasmy of deleted mtDNA without threshold and independently of deletion size. Biochimica et biophysica acta 1556(1): 41-52 (2002).
[45] Lin MT, Beal MF. Mitochondrial dysfunction and oxidative stress in neurodegenerative diseases. Nature 443(7113): 787-95 (2006).
[46] Schubert W, Prior R, Weidemann A, Dircksen H, Multhaup G, Masters CL, *et al.* Localization of Alzheimer beta A4 amyloid precursor protein at central and peripheral synaptic sites. Brain Res 563(1-2): 184-94 (1991).
[47] Roher AE, Esh CL, Kokjohn TA, Castano EM, Van Vickle GD, Kalback WM, *et al*. Amyloid beta peptides in human plasma and tissues and their significance for Alzheimer's disease. Alzheimers Dement 5(1): 18-29 (2009).
[48] Patel S, Shah RJ, Coleman P, Sabbagh M. Potential peripheral biomarkers for the diagnosis of Alzheimer's disease. Int J Alzheimers Dis 2011: 572495 (2011).
[49] Oddo S, Caccamo A, Shepherd JD, Murphy MP, Golde TE, Kayed R, *et al.* Triple-transgenic model of Alzheimer's disease with plaques and tangles: intracellular Abeta and synaptic dysfunction. Neuron 39(3): 409-21 (2003).
[50] Wang P, Yang G, Mosier DR, Chang P, Zaidi T, Gong YD, *et al.* Defective neuromuscular synapses in mice lacking amyloid precursor protein (APP) and APP-Like protein 2. J Neurosci 25(5): 1219-25 (2005).
[51] Akaaboune M, Allinquant B, Farza H, Roy K, Magoul R, Fiszman M, *et al.* Developmental regulation of amyloid precursor protein at the neuromuscular junction in mouse skeletal muscle. Mol Cell Neurosci 15(4): 355-67 (2000).
[52] Sarantseva SV, Kislik GA, Tkachenko NA, Vasil'ev AN, Shvartsman AL. [Morphological and functional abnormalities in neuromuscular junctions of Drosophila melanogaster induced by the expression of human APP gene]. Tsitologiia 54(5): 421-9 (2012).

[53] Gsell W, Conrad R, Hickethier M, Sofic E, Frolich L, Wichart I*, et al.* Decreased catalase activity but unchanged superoxide dismutase activity in brains of patients with dementia of Alzheimer type. J Neurochem 64(3): 1216-23 (1995).

[54] Habib LK, Lee MT, Yang J. Inhibitors of catalase-amyloid interactions protect cells from beta-amyloid-induced oxidative stress and toxicity. J Biol Chem 285(50): 38933-43 (2010).

[55] Radi R, Beckman JS, Bush KM, Freeman BA. Peroxynitrite oxidation of sulfhydryls. The cytotoxic potential of superoxide and nitric oxide. J Biol Chem 266(7): 4244-50 (1991).

[56] Yao J, Irwin RW, Zhao L, Nilsen J, Hamilton RT, Brinton RD. Mitochondrial bioenergetic deficit precedes Alzheimer's pathology in female mouse model of Alzheimer's disease. Proc Natl Acad Sci USA 106(34): 14670-5 (2009).

[57] Schuh RA, Jackson KC, Schlappal AE, Spangenburg EE, Ward CW, Park JH*, et al.* Mitochondrial oxygen consumption deficits in skeletal muscle isolated from an Alzheimer's disease-relevant murine model. BMC Neurosci 15: 24 (2014).

[58] Picard M, Hepple RT, Burelle Y. Mitochondrial functional specialization in glycolytic and oxidative muscle fibers: tailoring the organelle for optimal function. Am J Physiol Cell Physiol 302(4): C629-41 (2012).

[59] Kriketos AD, Pan DA, Sutton JR, Hoh JF, Baur LA, Cooney GJ*, et al.* Relationships between muscle membrane lipids, fiber type, and enzyme activities in sedentary and exercised rats. The Am J Physiol 269(5 Pt 2): R1154-62 (1995).

[60] Du H, Yan SS. Mitochondrial permeability transition pore in Alzheimer's disease: cyclophilin D and amyloid beta. Biochimica et Biophysica Acta 1802(1): 198-204 (2010).

[61] Foley P. Lipids in Alzheimer's disease: A century-old story. Biochimica et Biophysica Acta 1801(8): 750-3 (2010).

[62] Frisardi V, Panza F, Seripa D, Farooqui T, Farooqui AA. Glycerophospholipids and glycerophospholipid-derived lipid mediators: a complex meshwork in Alzheimer's disease pathology. Prog Lipid Res 50(4): 313-30 (2011).

[63] Ghosh M, Tucker DE, Burchett SA, Leslie CC. Properties of the Group IV phospholipase A2 family. Prog Lipid Res 45(6): 487-510 (2006).

[64] Fonteh AN, Chiang J, Cipolla M, Hale J, Diallo F, Chirino A*, et al.* Alterations in cerebrospinal fluid glycerophospholipids and phospholipase A2 activity in Alzheimer's disease. J Lipid Res 54(10): 2884-97 (2013).

[65] Yang X, Sheng W, He Y, Cui J, Haidekker MA, Sun GY*, et al.* Secretory phospholipase A2 type III enhances alpha-secretase-dependent amyloid precursor protein processing through alterations in membrane fluidity. J Lipid Res 51(5): 957-66 (2010).

[66] Kabarowski JH, Xu Y, Witte ON. Lysophosphatidylcholine as a ligand for immunoregulation. Biochem Pharmacol 64(2): 161-7 (2002).

[67] Sundaram JR, Chan ES, Poore CP, Pareek TK, Cheong WF, Shui G*, et al.* Cdk5/p25-induced cytosolic PLA2-mediated lysophosphatidylcholine production regulates neuroinflammation and triggers neurodegeneration. J Neurosci 32(3): 1020-34 (2012).

[68] Amtul Z, Uhrig M, Wang L, Rozmahel RF, Beyreuther K. Detrimental effects of arachidonic acid and its metabolites in cellular and mouse models of Alzheimer's disease: structural insight. Neurobiol Aging 33(4): 831 e21-31 (2012).

[69] Han X, Holtzman DM, McKeel DW, Jr. Plasmalogen deficiency in early Alzheimer's disease subjects and in animal models: molecular characterization using electrospray ionization mass spectrometry. J Neurochem 77(4): 1168-80 (2001).

[70] Wood PL, Mankidy R, Ritchie S, Heath D, Wood JA, Flax J*, et al.* Circulating plasmalogen levels and Alzheimer Disease Assessment Scale-Cognitive scores in Alzheimer patients. J Psychiat Neurosci 35(1): 59-62 (2010).

Received: May 23, 2014 **Revised: September 21, 2014** **Accepted: October 09, 2014**